Title

Modeling the emergence of viral resistance for SARS-CoV-2 during treatment with an anti-spike monoclonal antibody

Journal

PLOS Pathogens, 20(4)

ISSN

1553-7366

Authors

Phan, Tin
Zitzmann, Carolin
Chew, Kara W
et al.

Publication Date

2024

DOI

10.1371/journal.ppat.1011680

Peer reviewed

PLOS PATHOGENS

RESEARCH ARTICLE

Modeling the emergence of viral resistance for SARS-CoV-2 during treatment with an anti-spike monoclonal antibody

Tin Phan[1], Carolin Zitzmann[1], Kara W. Chew[2], Davey M. Smith[3], Eric S. Daar[4], David A. Wohl[5], Joseph J. Eron[5], Judith S. Currier[2], Michael D. Hughes[6], Manish C. Choudhary[7], Rinki Deo[7], Jonathan Z. Li[7], Ruy M. Ribeiro[1], Ruian Ke[1], Alan S. Perelson[1,8*], for the ACTIV-2/A5401 Study Team

1 Theoretical Biology & Biophysics, Los Alamos National Laboratory, Los Alamos, New Mexico, United States of America, **2** Department of Medicine, David Geffen School of Medicine, University of California, Los Angeles, California, United States of America, **3** Department of Medicine, University of California, San Diego, California, United States of America, **4** Lundquist Institute at Harbor-UCLA Medical Center, Torrance, California, United States of America, **5** Department of Medicine, University of North Carolina at Chapel Hill School of Medicine, Chapel Hill, North Carolina, United States of America, **6** Harvard T.H. Chan School of Public Health, Boston, Massachusetts, United States of America, **7** Department of Medicine, Division of Infectious Diseases, Brigham and Women's Hospital, Harvard Medical School, Boston, Massachusetts, United States of America, **8** Santa Fe Institute, Santa Fe, New Mexico, United States of America

* asp@lanl.gov

Citation: Phan T, Zitzmann C, Chew KW, Smith DM, Daar ES, Wohl DA, et al. (2024) Modeling the emergence of viral resistance for SARS-CoV-2 during treatment with an anti-spike monoclonal antibody. PLoS Pathog 20(4): e1011680. https://doi.org/10.1371/journal.ppat.1011680

Editor: Shuo Su, Nanjing Agricultural University, CHINA

Received: September 13, 2023

Accepted: March 18, 2024

Published: April 18, 2024

Data Availability Statement: Data are available under restricted access due to ethical restrictions as the data include potentially identifying information. Access to the data is governed by ACTG policy. Access can be requested by submitting a data request at https://submit.mis.s-3.net/ and will require the written agreement of the ACTG and the manufacturer of the investigational product. Requests will be addressed as per ACTG standard operating procedures. Completion of an ACTG Data Use Agreement may be required.

Abstract

To mitigate the loss of lives during the COVID-19 pandemic, emergency use authorization was given to several anti-SARS-CoV-2 monoclonal antibody (mAb) therapies for the treatment of mild-to-moderate COVID-19 in patients with a high risk of progressing to severe disease. Monoclonal antibodies used to treat SARS-CoV-2 target the spike protein of the virus and block its ability to enter and infect target cells. Monoclonal antibody therapy can thus accelerate the decline in viral load and lower hospitalization rates among high-risk patients with variants susceptible to mAb therapy. However, viral resistance has been observed, in some cases leading to a transient viral rebound that can be as large as 3–4 orders of magnitude. As mAbs represent a proven treatment choice for SARS-CoV-2 and other viral infections, evaluation of treatment-emergent mAb resistance can help uncover underlying pathobiology of SARS-CoV-2 infection and may also help in the development of the next generation of mAb therapies. Although resistance can be expected, the large rebounds observed are much more difficult to explain. We hypothesize replenishment of target cells is necessary to generate the high transient viral rebound. Thus, we formulated two models with different mechanisms for target cell replenishment (homeostatic proliferation and return from an innate immune response antiviral state) and fit them to data from persons with SARS-CoV-2 treated with a mAb. We showed that both models can explain the emergence of resistant virus associated with high transient viral rebounds. We found that variations in the target cell supply rate and adaptive immunity parameters have a strong impact on the magnitude or observability of the viral rebound associated with the emergence of resistant virus. Both variations in target cell supply rate and adaptive immunity parameters may explain why only some individuals develop observable transient resistant viral rebound. Our

Funding: This work was performed under the auspices of the US Dept. of Energy under contract 89233218CNA000001 and supported by NIH grant U54-HL143541 (RK), UM1AI068634, UM1AI068636 and UM1AI106701, and Los Alamos National Laboratory LDRD 20200743ER (RMR), 20200695ER (ASP), 20210730ER (RMR) and 20220791PRD2 (TP). The funders had no role in study design, data collection and analysis, decision to publish, or preparation of the manuscript.

Competing interests: We have read the journal's policy and the authors of this manuscript have the following competing interests: K.W.C. has received research funding to her institution from Merck Sharp & Dohme and consulted for Pardes Biosciences. D.M.S. has consulted for the following companies Fluxergy, Kiadis, Linear Therapies, Matrix BioMed, Lucira, VxBiosciences, Model Medicines, Bayer Pharmaceuticals, and Evidera. E. S.D. has consulted for Gilead, Merck, ViiV and Theratechnologies and received research funding to his institution from Gilead and ViiV. D.A.W. has consulted for Gilead Sciences, ViiV Healthcare, Janssen Pharmaceuticals, and Theratechnologies, and has university grant funding from Gilead Sciences, ViiV Healthcare, and Merck and Co. J. J. E. is on the DMC for Adagio/Invyvid and has consulted for Gilead Sciences and Merck & Co. J. S. C. has consulted for Merck & Co., J.Z.L. has consulted for Abbvie. The other authors have declared that no competing interests exist.

study highlights the conditions that can lead to resistance and subsequent viral rebound in mAb treatments during acute infection.

Author summary

Monoclonal antibodies have been used as a treatment for SARS-CoV-2. However, viral evolution and development of variants has compromised the use of all currently authorized monoclonal antibodies for SARS-CoV-2. In some individuals treated with one such monoclonal antibody, bamlanivimab, transient nasal viral rebounds of 3–4 logs associated with resistant viral strains occur. To better understand the mechanisms underlying resistance emergence with high viral load rebounds, we developed two different models that incorporate drug sensitive and drug resistant virus as well as target cell replenishment and fit them to data. The models accurately capture the observed viral dynamics as well as the proportion of resistant virus for each studied individual with little variation in model parameters. In the models with best-fit parameters, bamlanivimab selects for resistance mutants that can expand to high levels due to target cell replenishment. The ultimate clearance of virus however depends on the development of adaptive immunity.

Introduction

As of September 2023, SARS-CoV-2 has caused over 6.9 million deaths worldwide [1]. While vaccines are available to reduce disease severity, a large fraction of the world's population is not vaccinated [2]. With new variants that escape immunity rapidly emerging, effective treatment for severe cases is urgently needed [3]. Anti-SARS-CoV-2 monoclonal antibodies (mAbs) represent one class of effective treatments [4]. For example, the first monoclonal antibody that received emergency use authorization (EUA) for the treatment of SARS-CoV-2, bamlanivimab (BAM), can accelerate the viral decline and lower hospitalization and death rates among high-risk patients [5,6].

One concerning observation during treatment of SARS-CoV-2 infection with mAbs is the emergence of viral resistance and concomitant viral rebound. In the case of BAM treatment, after the initial peak in the viral load, viral rebounds of up to 3–4 orders of magnitude consisting mostly of resistant virus have been observed in small subsets of patients in multiple studies [7–9]. During rebound, infectious viruses are culturable, implying virus may be able to be transmitted and infect others [10].

Since mAbs are a treatment for SARS-CoV-2 and other viral infections such as respiratory syncytial virus and Ebola virus [11], understanding the mechanisms that allow resistant virus to emerge and rebound is important for designing effective treatment strategies that reduce disease severity and the chance of on-treatment viral transmission. Furthermore, such analyses can provide insights on the underlying dynamics of SARS-CoV-2 infection, such as the impact of the host target cell regeneration and adaptive immune responses on viral rebound, which has potential implications for the development of the next generation of mAb therapies and viral rebound after nirmatrelvir-ritonavir or other antiviral therapies [12–16].

Here, we use data from the ACTIV-2/A5401 randomized controlled clinical trial (NCT04518410) of BAM [5,7] to investigate the mechanism that gives rise to the observed transient viral rebound associated with the emergence of resistant virus. BAM is an IgG1 monoclonal antibody that binds to the SARS-CoV-2 virus's spike protein, blocking its ability

to enter and infect target cells. Due to its high potency for neutralizing SARS-CoV-2 [5,6], BAM can select for escape mutations such as E484K, an emergent mutation observed in the majority of rebound cases [7–9]. As a single substitution mutation, E484K is likely to be present at low frequencies at the time of treatment initiation and selected for in the presence of BAM (see Section A in S1 Text), yet only a small fraction of treated patients shows signs of resistance emergence and transient viral rebound [7]. The selective pressure of BAM is likely the reason why some resistant mutations become dominant during the transient viral rebound; however, there must be other important factors associated with high viral load rebound.

Drug resistance to antiviral treatments has been studied extensively for many viral pathogens [17–21]. Rapid viral growth under treatment requires high resistance of the virus and the availability of abundant target cells for the resistant virus to replicate and spread further as discussed in Ke et al. [21]. Without enough target cells, the selected resistant virus is unlikely to generate an observable transient viral rebound. For SARS-CoV-2, it has been shown that the viral load peaks around the time of or a few days after symptom onset [22–25], suggesting cells that are available for early infection either become depleted (by infection) or protected by innate immune responses [22] causing the virus to fall post-peak. The fact that the emergence of resistant virus associated with high viral load rebound occurs several days post symptom onset in some patients treated with BAM [7] is, therefore, difficult to explain.

Mathematical models are well suited to study the phenomenon of drug resistance and viral rebound [19–21,26–29]. We hypothesized the replenishment of target cells is necessary to generate the high transient viral rebound. Thus, to better understand the crucial factors leading to the emergence of resistant virus associated with high viral load rebound, we built models that include feasible mechanisms that can increase the availability of potential virus producing cells: the natural proliferation of target cells such as epithelial cells expressing the ACE-2 receptor [30] and the loss of protection from infection by the innate immune response [31] and fit these models to data from individuals who experienced viral rebound due to the emergence of resistant virus during BAM treatment.

Methods

Ethics statement

This research was approved by the LANL Human Subjects Research Review Board (HSRRB)

Data. We analyzed data from the cohort of individuals with SARS-CoV-2 infection and symptoms consistent with COVID-19 who were given a single infusion of 700 mg BAM in a phase 2 randomized, placebo-controlled trial (ACTIV-2/A5401 study) described in detail previously [5,7]. Viral load and mutant frequency data were obtained from anterior nasal swabs collected by the participants daily from the time of the BAM infusion to day 14 and at days 21 and 28. There were eight individuals who showed viral rebound with emerging resistance mutations in this treatment group. Patient B2-10, who showed signs of transient viral rebound with mutation S494P, only had four data points above the quantifiable limit and only one data point associated with the S494P resistance. Hence, we focus our study on the other seven participants with more frequent data (B2-2 to B2-8), who exhibited transient viral rebound associated with resistant mutants.

Models. Classical target cell limited models with a single viral population have been used to study within-host dynamics of SARS-CoV-2 [28,32–38] and other diseases such as HIV and HCV [39,40]. Since our data set contains data on both the viral load and the frequency of resistant mutants, we used a two-strain SARS-CoV-2 model to utilize both types of data [20]. In this model, target cells (T) represent the epithelial cells expressing ACE-2 receptors that are

susceptible to infection. The target cell dynamics is governed by

$$\frac{dT}{dt} = -\beta_1 V_1 T - \beta_2 V_2 T. \tag{1}$$

We classify SARS-CoV-2 viruses as either sensitive (V_1) or resistant (V_2) to BAM. Note that V_1 and V_2 do not indicate two particular genotypes of SARS-CoV-2, but rather groups of viruses that are either sensitive or resistant to BAM. The other equations defining the model are:

$$\begin{aligned}
\frac{dE_1}{dt} &= \beta_1 V_1 T - kE_1 \\
\frac{dE_2}{dt} &= \beta_2 V_2 T - kE_2 \\
\frac{dI_1}{dt} &= kE_1 - \delta(t) I_1 \\
\frac{dI_2}{dt} &= kE_2 - \delta(t) I_2 \\
\frac{dV_1}{dt} &= \pi(1-\mu) I_1 - cV_1 \\
\frac{dV_2}{dt} &= \pi I_2 + \mu\pi I_1 - cV_2.
\end{aligned} \tag{2}$$

In this model, viruses V_1 and V_2 infect target cells at rate β_1 and β_2, respectively. The infection produces E_1 and E_2, which are cells infected by V_1 and V_2, respectively, in the eclipse phase of the viral lifecycle and not yet producing virus. Cells in the eclipse phase move into productive infection with rate k. Thus, after staying in the eclipse phase for an average duration of $1/k$, infected cells start producing viruses at rate π and are reclassified as productively infected cells, I_1 and I_2, respectively. We also allow for a fixed mutation rate μ from the BAM sensitive to BAM resistant virus. Infected cells and viruses are cleared at per capita rates $\delta(t)$ and c, respectively. The loss rate of infected cells also includes the emergence of adaptive immunity, which is modeled as in the study by Pawelek et al. [41] by

$$\delta(t) = \begin{cases} \delta, t < t^* \\ \delta_M - (\delta_M - \delta) e^{-\sigma(t-t^*)}, t \geq t^* \end{cases}. \tag{3}$$

We define δ and δ_M as the baseline and maximum death rates of the infected cells, respectively. For simplicity, we set $\delta_M = 10\delta$. Time t^* is when adaptive immunity starts to emerge and σ determines the emergent speed of adaptive immunity. Note that adaptive immunity affects the cells infected by either viral strain.

Neutralizing effect and dynamics of neutralizing antibodies. We explicitly incorporate the passive infusion and decay dynamics of BAM based on the model developed by [42]. We let $A(t)$ be the serum concentration of BAM with unit $\mu g\ mL^{-1}$. We define t_{inf} as the time after infection that BAM infusion starts, ΔT as the duration of the infusion (assumed to be 1 hour or 1/24 day), and A_{max} as the maximum serum concentration (taken from data for these seven

study participants). The equation governing the antibody dynamics takes the form

$$A(t) = \begin{cases} 0, t < t_{inf} \\ \frac{A_{max}}{\Delta t}\left(t - t_{inf}\right), t_{inf} \leq t < t_{inf} + \Delta t \\ A_{max} e^{-\alpha\left(t-\left(t_{inf}+\Delta t\right)\right)}, t > t_{inf} + \Delta t \end{cases}. \quad (4)$$

For each study participant, we have the maximum antibody concentration (A_{max}) and the concentration at day 28(A_{28}). By fitting an exponential decay function that goes through the data points A_{max} and A_{28} we estimate the decay rate α (Table A and Section B in S1 Text). Note that we do not include a loss term for $A(t)$ due to the binding to the viruses or a gain term when the antibody dissociates from an immune complex. This is a simplification based on the observation that 99% of individuals infused with BAM have mAb concentrations greater than the IC90 (the concentration required for 90% inhibition) 28 days after the infusion [5]. Thus, antibodies are in great excess, and we assume the mAb concentration is not noticeably affected by interaction with the virus.

The neutralizing effect of BAM is modeled as follows. Antibodies bind to sensitive and resistant viruses at rates $k_{on,1}$ and $k_{on,2}$, respectively, to create neutralized virus-antibody immune complexes C_1 and C_2, respectively, which are no longer able to infect target cells. The complexes dissociate at rates $k_{off,1}$ and $k_{off,2}$ and are cleared at rates γ_1 and γ_2, respectively for the sensitive and resistant viruses. This leads to the following modifications to the basic target cell limited model.

$$\begin{aligned} \frac{dV_1}{dt} &= \pi(1-\mu)I_1 - k_{on,1}V_1A + k_{off,1}C_1 - cV_1 \\ \frac{dC_1}{dt} &= k_{on,1}V_1A - k_{off,1}C_1 - \gamma_1 C_1 \\ \frac{dV_2}{dt} &= \pi I_2 + \pi\mu I_1 - k_{on,2}V_2A + k_{off,2}C_2 - cV_2 \\ \frac{dC_2}{dt} &= k_{on,2}V_2A - k_{off,2}C_2 - \gamma_2 C_2. \end{aligned} \quad (5)$$

Together, Eqs (1)–(5) constitute the basic viral dynamic model with the neutralizing effect of antibodies. The E484K mutation, which is observed in 5 out of the 7 participants with transient viral rebound, is an escape mutant that abrogates BAM binding. A previous in vivo study showed that the binding affinity of BAM to the E484K spike protein is less than 1% of the binding to wild type SARS-CoV-2 [43]. Hence, we assume $k_{on,2}$ is negligible, and thus we do not account for the dynamics of C_2.

Our first intuition is perhaps to attribute the observed viral rebound solely to resistance to BAM as the majority of rebound viruses are resistant mutants. However, the timing of viral rebound suggests a greatly reduced pool of target cells at the time of BAM treatment, which was a median of 4.5 days post-symptom onset for the seven individuals analyzed. Thus, a mechanism for a supply of target cells is needed to support the rebound (See Sections A and C in S1 Text). We investigate two non-mutually exclusive mechanisms that may contribute to the availability of target cells after peak viral load, i.e., proliferation of target cells [30,44,45] and transition of cells from an interferon induced antiviral state back to a susceptible state due to a decline in the level of type I and III interferons [31,46,47]. Thus, we introduce the modifications needed for each proposed mechanism to explain the rebound of virus.

Target cell regeneration (the logistic proliferation model). We assume homeostatic mechanisms induce a logistic growth of target cells that attempts to restore the population size to its baseline level. This leads to the following modification of the target cell dynamics:

$$\frac{dT}{dt} = -\beta_1 V_1 T - \beta_2 V_2 T + rT\left(1 - \frac{T + E_1 + E_2 + I_1 + I_2}{T_M}\right), \tag{6}$$

where r and T_M are the maximum proliferation rate (or regeneration rate) and carrying capacity, respectively. While it may be possible for infected cells to proliferate and generate infected progeny, existing experimental evidence suggests that proliferation of cells infected with SARS-CoV-2 is impaired [48–50]. Hence, we assume proliferation of infected cells is negligible.

Loss of the antiviral state (the innate immune response model). The protective effect of the type-I and type III interferons (representative of the innate immune response) is modeled as in previous studies [22,41,51]. We introduce a variable R that keeps track of cells in an antiviral state and thus refractory to infection. This leads to the following changes to the original model:

$$\begin{aligned} \frac{dT}{dt} &= -\beta_1 V_1 T - \beta_2 V_2 T - \phi(I_1 + I_2)T + \rho R \\ \frac{dR}{dt} &= \phi(I_1 + I_2)T - \rho R. \end{aligned} \tag{7}$$

In this formulation, we assume the interferon level is proportional to the number of productively infected cells, so the rate of conversion of target cells to refractory cells is given by the rate constant ϕ multiplied by the total number of infected cells, (I_1+I_2). The refractory cells return to being susceptible to infection at per capita rate ρ.

Population fitting. We used a nonlinear mixed effects modeling approach (software Monolix 2021, Lixoft, SA, Antony, France) to fit each model to the viral load and mutant frequency data for all individuals simultaneously. In this approach we fit all the data simultaneously, both total viral load and fraction of resistant virus, across all individuals, increasing the power to estimate the model's quality of fit to the data. Note that we fit the distribution of each parameter (mean and variance) rather than just point estimates. More details of the procedure and the use of Monolix can be found in [52]. Specifically, here, besides fitting the total viral load (V + C in the model), we fit $\frac{V_1}{V_1+V_2}$ to the frequency of the BAM sensitive viral population. We do not fit $\frac{V_2}{V_1+V_2}$ to the frequency of the BAM resistant viral population because it is simply $1 - \frac{V_1}{V_1+V_2}$, so the resistance data is colinear with the sensitive data. Comparison of the models was done using the corrected Bayesian Information Criterion (BICc) [53,54] as reported by Monolix and is given by:

$$\text{BICc} = -2LL + \dim(\theta_R)\log N + \dim(\theta_F)\log n_{tot},$$

where -2LL is the -2 times loglikelihood, dim θ_R is the number of the random and fixed covariate parameters, N is the number of subjects, dim (θ_F) is the number of fixed effects (except covariates), and n_{tot} is the total number of observations (Monolix.lixoft.com/tasks/log-likelihood-estimation).

Since we do not know the time of infection and estimating the time of infection without data during the early phase of infection is problematic due to model identifiability issues [55,56], we fixed the duration from infection to symptom onset to 5 days as in previous studies [34,57,58]. This assumption is based on estimates that the duration from exposure to symptom

onset is about 5 days [24,59–62]. Furthermore, fixing the duration from infection to symptom onset allows us to focus on our objective, which is to access potential mechanisms that contribute to transient viral rebound of resistant virus.

For all models, we fixed the initial number of target cells $T(0)$ to 8×10^7 cells [22]. This is an estimate based on the observation that the number of epithelial cells that expresses the ACE-2 receptor is roughly 20% of the epithelial cells in the upper respiratory tract (around 4×10^8 cells) [63]. For the logistic proliferation model, we set $T_M = T(0)$.This means in the absence of viral infection, the proliferation rate is negligible, which is consistent with observation that the turnover of epithelial cells is on the order of months; however, the proliferation rate is accelerated following acute infection [44].

As we do not know the number of viruses that initiate infection, we use a method suggested by Smith et al. [64] in which we assume the initiating virus is either cleared or rapidly infects cells. Thus, we initiate infection by setting $E_1(0) = 1$ cell. In a previous SARS-CoV-2 modeling study [22] we showed that choosing larger values of $E_1(0)$ such 5 or 10 cells led to slightly larger Akaike Information Criterion values, justifying our choice of $E_1(0) = 1$ cell. Also, besides resistance arising by viral mutation there can be baseline resistance. Hence, we fit $E_2(0)$ and keep track of the first time, t^{**}, the model predicts $E_2(t^{**}) \geq 1$, where t^{**} marks a physiologically relevant threshold for the emergence of resistance virus that can be compared across individuals.

We fixed the rate constant for BAM binding to the SARS-CoV-2 spike protein k_{on} to 5.5×10^5 M^{-1} s^{-1} and the rate constant for unbinding k_{off} to 2.5×10^{-5} s^{-1} [65]. This gives an equilibrium dissociation constant (K_D) of 0.045 nM, which is somewhat less than the reported value of 0.071 nM in the EUA for BAM [65]. Due to the BAM concentration being given in units of ug/mL and the rate parameter k_{on}, being given in inverse molar units, we converted the BAM concentration into molar units using its molecular weight of 1.46 x10^5 Da, yielding 1 ug/mL = 6.85×10^{-9} M.

The rate of exit from the eclipse phase, k, is fixed to 4 per day and the viral clearance rate, c, is fixed to 10 per day [22]. BAM accelerates viral clearance within three days of infusion [5] and thus we expect immune complexes to be cleared faster than free virus. Therefore, we carried out sensitivity tests with γ, the rate of immune complex clearance, varying between c and $5 \times c$ based on the observation that neutralizing antibody enhances HIV-1 clearance by $\sim$3-fold [66]. We found that model fits were relatively insensitive to the value of γ in this range and we fixed the clearance rate of the virus-antibody immune complexes to $3 \times c$ (see Table B and Section D in S1 Text), the value found by Igarashi et al. [66]. The mutation rate μ was fixed to 10^{-6} per day [67,68]. Finally, we constrained the infection rate constant for the resistant virus β_2 to be less than β_1 as we expect the resistance virus to be less fit than the wildtype. A complete summary of parameters is presented in Table C and Section E in S1 Text.

Results

To demonstrate that target cell replenishment is necessary, we fit a target cell limited model given by Eqs (1)–(5) to the data. The results of such fit are inconsistent with previous observations about when the viral load peak occurs. The model can recapitulate the second peak, i.e. the rebound, but at the time of treatment, the model predicts that the viral load has yet to reach its normal first peak in all seven participants (Fig A and Section C in S1 Text). This is unlikely since the viral peak is usually around the time of symptom onset and BAM was initiated a median of 4.5 days post symptom onset in these participants [7]. Essentially, this simple model tries to preserve target cells to allow the resistant virus to grow by preventing the viral

load from increasing rapidly after infection. Hence, we proceeded with testing models that include target cell replenishment.

The logistic proliferation model

We first tested the logistic proliferation model, which incorporates proliferation of target cells (see Methods). Fitting the model to data, we found that the model can describe the emergence of resistant virus reasonably well (Fig 1). Model simulation using the best-fit parameter values recapitulated the observation that the drug sensitive viral population (green in Fig 1) was the dominant strain in all seven study participants before treatment. After BAM infusion, the sensitive viral population was rapidly replaced by the resistant viral population (red in Fig 1), which expanded and led to the observed viral rebound.

The parameter estimates for the logistic proliferation model are relatively consistent across participants (Table 1). The one exception is the time that the resistant virus emerges t^{**}. Participant B2-2 had an estimated resistance emergence time that was much earlier (0.84 days) than the other six participants (range 3.3 to 4.8 days). This, however, is consistent with experimental data, which showed B2-2 had baseline (at the time of BAM infusion) BAM resistance mutations E484K and E484Q. For this individual, the anterior nasal swab data (which is used for the fitting), showed baseline mutation frequencies of less than 10%. However, in nasopharyngeal swabs, which were taken much less frequently and hence not used for model fitting, the frequency of the BAM resistance mutation E484K was over 60% at baseline [7]. No baseline mutation was detected in the other six participants in either anterior nasal or nasopharyngeal measurements, which is consistent with the late predicted emergence time of the resistant viral population.

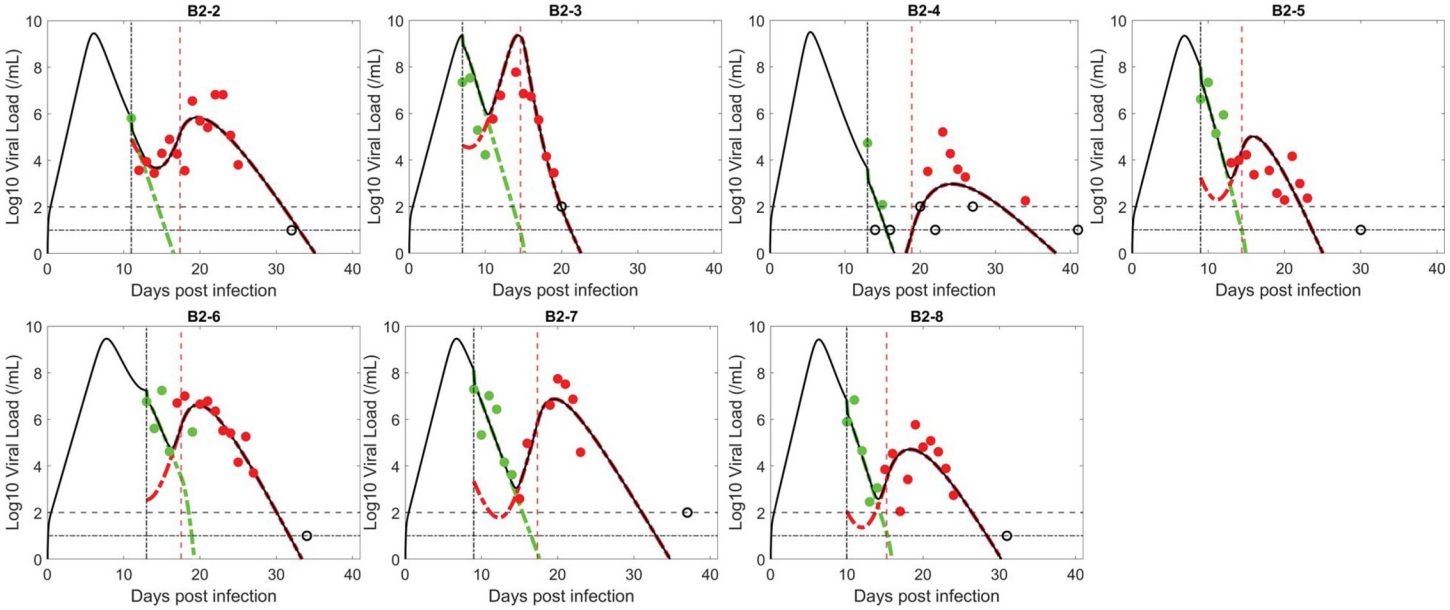

Fig 1. Fit of the logistic proliferation model to the data. The circles represent viral load data which are filled green when the viral population was dominated by BAM sensitive virus and filled red when dominated by resistant virus. The unfilled circles are data below the limit of quantification (2 $\log_{10}$ RNA copies/mL) or limit of detection (1.4 $\log_{10}$ RNA copies/mL, indicated by horizontal lines). Black curves show the best-fit of the model to the total viral load. When plotting the model fit, V_1 (BAM sensitive) is represented by a dashed–green curve and V_2 (BAM resistant) by a red curve. The vertical black line indicates the time of treatment initiation. The vertical red line indicates the estimated time, t^* when adaptive immunity begins to emerge.

https://doi.org/10.1371/journal.ppat.1011680.g001

Table 1. Best fit parameters for the logistic proliferation model.

	B2-2	B2-3	B2-4	B2-5	B2-6	B2-7	B2-8
$-log_{10}(\beta)$ ($mL\ RNA\ copies^{-1}\ day^{-1}$)	8.84	8.90	8.76	8.86	9.01	8.91	8.85
β_2/β_1	0.99	0.99	0.99	0.99	0.99	0.99	0.99
δ (day^{-1})	2.22	2.57	2.18	2.90	1.81	2.04	2.38
π ($RNA\ copies\ mL^{-1}\ day^{-1}$)	1174.51	1176.53	1176.53	1172.40	1174.33	1173.98	1176.50
t^{**} ($days$)	0.84	4.40	3.29	4.27	4.82	4.17	3.91
r (day^{-1})	0.61	0.89	0.64	0.91	0.89	0.86	0.84
σ (day^{-1})	0.26	0.33	0.22	0.28	0.25	0.30	0.21
t^* ($days$)	17.38	14.63	18.89	14.40	17.53	17.35	15.23

https://doi.org/10.1371/journal.ppat.1011680.t001

The innate immune response model

Next, we tested the ability of the innate immune response model in which target cells arise from the loss of the antiviral state to fit the observed data (see Methods). The model assumes type-I and type-III interferons levels are proportional to the number of infected cells, and that these interferons put target cells into an antiviral state that is refractory to viral infection [31,69,70]. The antiviral state is not permanent, and the model assumes refractory cells return to being susceptible to infection at a constant rate. As the viral infection progresses, more cells become infected, more interferon is produced, and a larger number of target cells become refractory to infection. However, after the viral load reaches its peak, both the viral load and the number of infected cells decline. As the number of infected cells and interferon levels decline, fewer target cells become protected, while cells in the refractory state lose protection and return to being susceptible to infection. The refractory cells returning to target cells can provide resistant virus with the necessary resource to rebound.

Similar to the logistic proliferation model, the innate immune response model can also capture the emergence of resistant virus and the observed transient viral rebound (Fig 2). The model also describes well the quantitative dynamics of both the BAM sensitive and resistant viral populations and the observation that prior to treatment, the sensitive virus is dominant, while, after BAM infusion, the resistant viral population rapidly replaces the sensitive one, before finally being cleared by adaptive immunity (Fig 2).

The estimated parameters in the innate immune response model are consistent across patients (Table 2). Interestingly, the estimated viral dynamics parameters that are common to both the logistic proliferation and innate response models are very similar (e.g., β, π, and δ). Furthermore, the best estimates of the ratio β_2/β_1, in both models, are close to the upper bound of 1, which suggests BAM resistance mutations, such as E484K, have little fitness cost. The estimated emergence times of the resistant virus for the innate immune response model follow similar trend to that of the logistic proliferation model, which reflects the observation of a baseline mutation in B2-2 but not the other participants. The estimated values for ρ are consistent with the expected duration of protection of refractory cells [31,46,47,71].

We compare the data support for each model using the negative log-likelihood (-2LL) and the corrected Bayesian Information Criterion (BICc) for both models (Table 3). The innate immune response model fits the data slightly better than the logistic proliferation model

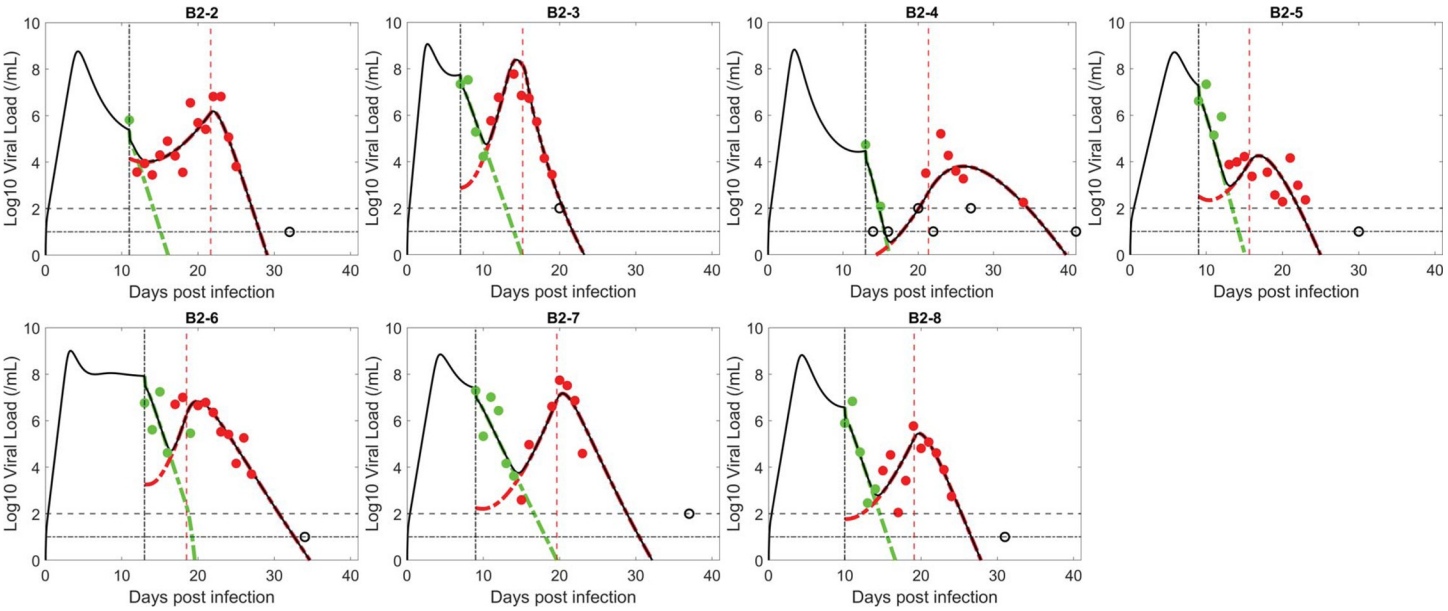

Fig 2. Fit of the innate immune response model to the data. The circles represent viral load data which are filled green when the viral population was dominated by BAM sensitive virus and filled red when dominated by resistant virus. The unfilled circles are data below the limit of quantification or limit of detection (indicated by horizontal lines). Black curves show the best-fit of the model to the total viral load. When plotting the model fit, V_1 (BAM sensitive) is represented by a dashed–green curve and V_2 (BAM resistant) by a red curve. The vertical black line indicates the time of treatment initiation. The vertical red line indicates the estimated time, t^*, when adaptive immunity begins to emerge.

https://doi.org/10.1371/journal.ppat.1011680.g002

(lower fitting error); however, the logistic proliferation model is slightly preferred based on BICc, because the innate immunity model has one more model parameter, which is two more estimated parameters since population fitting estimates a mean and a standard deviation for the parameter.

Adaptive immunity is crucial in viral clearance. In a target cell limited model (see Section C in S1 Text), the constant depletion of target cells ultimately leads to the decline in viral

Table 2. Best fit parameters for the innate immune response model.

	B2-2	B2-3	B2-4	B2-5	B2-6	B2-7	B2-8
$-log_{10}(\beta)$ ($mL\ RNA\ copies^{-1}\ day^{-1}$)	8.61	8.20	8.40	8.79	8.39	8.67	8.63
β_2/β_1	0.98	0.98	0.99	0.99	0.99	0.86	0.98
δ (day^{-1})	2.38	2.19	3.59	2.75	2.32	1.55	2.26
π ($copies\ mL^{-1}\ day^{-1}$)	1097.54	1102.81	1102.53	1102.11	1108.76	1100.88	1102.17
ϕ ($cells^{-1}\ day^{-1}$)	8.1e-07	9.5e-07	8.1e-07	4.8e-07	7.5e-07	7.8e-06	6.9e-07
ρ (day^{-1})	0.021	0.069	0.021	0.1	0.15	0.053	0.04
t^{**} ($days$)	0.77	1.61	2.24	3.87	2.04	2.96	2.85
σ (day^{-1})	0.32	0.65	0.038	0.12	0.27	0.41	0.31
t^* (day)	21.65	15.16	21.37	15.66	18.48	19.65	19.1

https://doi.org/10.1371/journal.ppat.1011680.t002

Table 3. Comparison of fitting between the logistic proliferation and innate immune response models. Bolded text shows the smaller value.

	-2LL	*BICc*
Logistic proliferation model	191.59	**260.63**
Innate immune response model	**190.68**	267.02

https://doi.org/10.1371/journal.ppat.1011680.t003

load; however, both the logistic proliferation model and the innate immune response model contain mechanisms that can replenish the pool of target cells. In a logistic proliferation model without adaptive immunity, the production of target cells makes it possible for virus to oscillate or be sustained indefinitely (see Fig B and Section F in S1 Text). In the innate immune response model without adaptive immunity, the dynamics of target cells going in and out of the refractory state can also give rise to oscillations and the possibility of a slowly decreasing viral load (see Fig B and Section F in S1 Text). Thus, for these models to generate dynamics consistent with the observed data with rapid ultimate virus clearance, adaptive immunity must be included in both models.

Variations in individual characteristics may explain why only some participants develop resistance with high transient viral rebound

A previous study using a similar innate immune response model for SARS-CoV-2 infection but fit to a different set of data from untreated, unvaccinated individuals estimated $\phi = 3.4 \times 10^{-6}$ cells^{-1} day^{-1} and $\rho = 0.004$ /day (mean of the estimates for all individuals studied) [22]. Compared to these estimates, our estimate for $\phi = 8.1 \times 10^{-7}$ cells^{-1} day^{-1} is slightly smaller, but within one order of magnitude; however, our estimate for $\rho = 0.053$ /day is at least one order of magnitude larger. This would indicate that the rate of reversal of the refractory state, ρ, is much faster in the rebound individuals. To support this, we fitted the n = 102 individuals in this trial treated with 700 mg BAM, and who did not rebound, as well as the n = 160 individuals in the control group given a placebo (Figs C-G and Section G in S1 Text). In those two groups, without viral rebound associated with resistance, the reversal rate from the refractory state, ρ, was much smaller than in the individuals who rebounded (Figs H-I and Section G in S1 Text). Specifically, the values for ϕ are 1.48×10^{-6} (treated non-rebound) and 1.05×10^{-6} cells^{-1} day^{-1} (placebo) and the values for ρ are 0.003 /day (treated non-rebound) and 0.002 /day (placebo). This difference in the rate that refractory cells lose protection, ρ, along with the ability of BAM to neutralize wildtype virus may explain why the viral trajectories for these seven study participants exhibit high transient viral rebound of resistant virus [7].

To study this further, we used the best fit parameters for B2-8 and simulated the effect of decreasing the supply rate of target cells, r (the logistic proliferation model) or the rate cells lose their antiviral state ρ (the innate immune response model). We found that decreasing the maximum target cell proliferation rate r in the logistic proliferation model caused the magnitude of the transient viral rebound to diminish (Fig 3A). Reducing the rate that refractory cells return to the target cell pool ρ also has a similar effect (Fig 3B). However, there is a distinction in the qualitative effect of the two mechanisms. The proliferation term creates new target cells to compensate for the number of cells lost, while the refractory term only stores target cells in an antiviral state temporarily and then returns them to the target cell state without creating new target cells. These results suggest that how quickly target cells become available during infection may be a key factor determining the magnitude of the transient viral rebound associated with the emergence of resistant virus. Since these parameters vary among individuals, it may explain why only some individuals exhibit high resistant viral rebound following

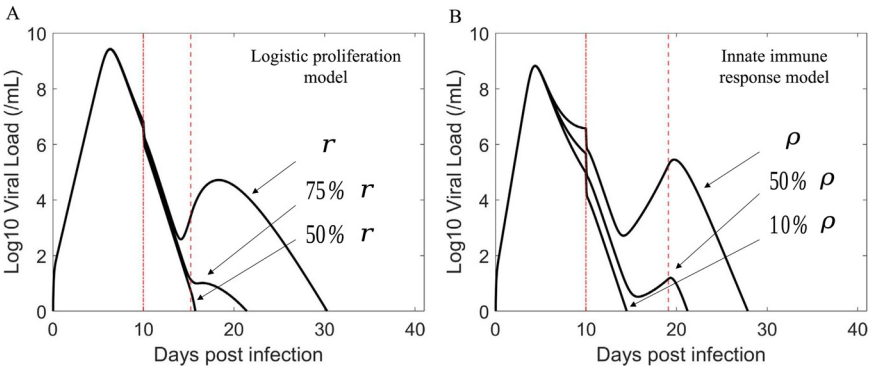

Fig 3. The rate of target cell replenishment has a crucial role in driving the amplitude of the viral rebound. Baseline parameters for the simulation are taken from the best fit parameters of B2-8. The first vertical red (dashed dot) line indicates the time of treatment initiation. The second vertical red (dashed) line indicates when adaptive immunity begins to emerge. (A) Viral rebound is more likely to be observable (e.g., sufficiently high VL) with increasing intrinsic growth rate *r*. (B) Viral rebound is more likely to be observable with increasing rate of refractory cells returning to cells susceptible to infection ρ.

https://doi.org/10.1371/journal.ppat.1011680.g003

treatment with BAM. Additionally, differences in mutations in spike, differences in BAM binding kinetics, differences in BAM concentration in different treated individuals, differences in the time BAM was given relative to time of infection, differences in viral kinetics, and in particular higher viral load at the time of BAM treatment in participants with treatment-emergent resistance than those who did not develop resistance [7], etc. may further contribute to the observation that only a small fraction of treated individuals develop resistance and transient viral rebound.

Discussion

The emergence of BAM resistant viral mutants associated with transient viral rebounds of 3–4 viral logs has been observed in some individuals treated with BAM [7–9]. While the emergence of resistant viral mutants can be attributed to the selective pressure of BAM, the 3–4 log increase in viral load is also likely dependent upon having an additional supply of target cells. Viral dynamic models without target cell replenishment are suitable to describe acute infection [37,72]. However, we found that simple target cell limited models were not consistent with the data (Fig A and Section C in S1 Text). To observe the large increase in viral load with the emergence of resistance, such models predict treatment takes place early during infection (before the peak in viral load), which was not the case here. To reconcile these contradicting observations and to better understand the factors leading to the emergence of resistant virus with high transient viral rebound, we developed two models with different underlying mechanisms that allow for target cell replenishment during the infection.

In an acute infection, target cells production is often assumed to be negligible due to the short duration of the infection—continued viral infection is then dependent upon the availability of target cells [28]. However, emerging resistant virus with viral rebound extends the duration of infection, which may justify the inclusion of target cell proliferation in the model. Previous SARS-CoV-2 models examined the effect of proliferation of target cells, but not in light of the emergence of resistance and transient viral rebound [73–78]. We showed that by incorporating a logistic proliferation term into a two-viral population viral dynamic model with adaptive immunity, the model can describe the emergence of resistant virus, which leads to the high transient viral rebound following treatment with BAM (Fig 1). This result echoes a

previous observation that in mice with influenza, stimulation of alveolar type II cells prior to infection can increase the number of alveolar epithelial cells expressing ACE-2 receptors and enhance infection [79].

Upon viral infection, infected cells as well as plasmacytoid dendritic cells (not modeled), release type-I and type-III interferons, which put neighboring target cells into an antiviral state, protecting them from viral infection [31,69,70,80]. Thus, a strong interferon response correlates with strong suppression of viral replication [81]. Previous modeling efforts have captured these effects in a different context [22,41,82]. However, over time, refractory cells likely lose their antiviral state [31,46,47]. Thus, if there are sufficient numbers of cells in the refractory state and these return to being susceptible to infection, then the returning cells would contribute to a late increase in the pool of susceptible cells. In this case, if individuals were treated with an mAb that effectively neutralizes the sensitive virus, then it would create an opportunity for the resistant virus to infect the increasing number of target cells, allowing the vigorous growth of resistant virus associated with an observable transient viral rebound.

SARS-CoV-2 may be able to antagonize the initial innate immune response by inducing lower production of type I and III interferons as compared to other respiratory viruses, which has been linked to the severity of SARS-CoV-2 disease [83]. However, the importance of type-I interferons in SARS-CoV-2 infection has been highlighted by the finding that at least 10% of people with life-threatening COVID-19 pneumonia had neutralizing auto-antibodies against type I interferon [84]. There is also a sharp increase in the presence of such antibodies with age in the elderly and people with these auto-antibodies account for at least 18% of all COVID-19 fatalities [85]. There has also been an association found between various single nucleotide polymorphisms in interferon λ genes 3 and 4 and COVID-19 disease severity [86,87] again highlighting the protective role of an interferon response.

Two SARS-CoV-2 studies using a murine model [88,89] suggested that innate immunity may only have a minimal role in viral clearance, while adaptive immunity significantly contributes to the ultimate clearance of acute infection. A recent clinical study also echoed this result by examining the role of CD4+ T-cells in shaping the antiviral activity of the immune response [90]. We have also shown that the inclusion of adaptive immunity in our models is crucial for viral clearance (Fig B and Section F in S1 Text).

The supply rate of target cells should have a strong impact on the magnitude of the transient viral rebound of resistant virus, or whether the emergence of resistant virus is observable clinically. We examined this effect by varying the target cell supply rate in both models. Fig 3 confirmed our speculation. This suggests that how quickly target cells become available during infection may be a key factor along with BAM driving the high transient viral rebound of resistant virus. Because the target cell supply rate most likely varies among individuals, this may help explain why only some individuals treated with BAM develop observable resistant viral rebound. The innate immune response model predicts that the rapid reduction in infected cells due to BAM led to a reduction in the production of type-I and type-III interferons. With less interferon fewer target cells are converted into the refractory state. In this scenario, if the rate that refractory cells return to susceptible cells is sufficiently fast, it would lead to a sizable increase in the number of target cells that allow for the resistant virus to emerge to an observable population size. This hypothesis is consistent with the observation that the rate that refractory cells return to susceptible cells for rebound participants is much faster than non-rebound participants (Figs H-I and Section G in S1 Text). While BAM selects for resistant viral population, target cell replenishment drives the amplitude of the transient viral rebound. See Fig 4 for a summary description of our results.

In addition to the above two mechanisms, we also examined the possibility of antibody-dependent enhancement (ADE) extending the range of cells that are targets of infection.

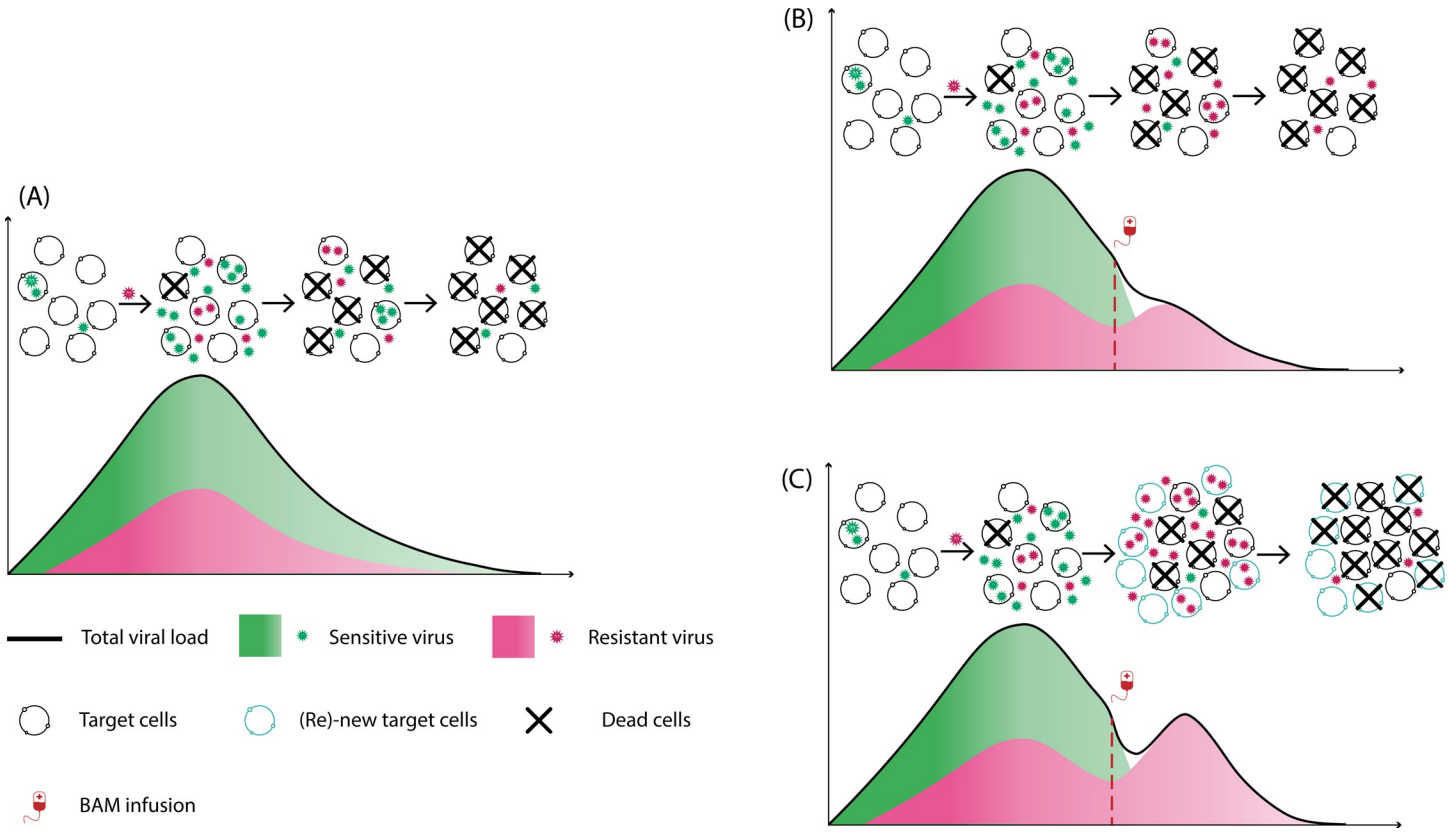

Fig 4. Target cell replenishment can explain the emergence of resistant virus associated with high transient viral rebound. (A) Natural course of acute infection as described by a standard viral dynamic model. (B) Without target cell replenishment, the resistant virus becomes the dominant population but does not lead to observable transient viral rebound. (C) Target cell replenishment–either via new production or target cell returning from the refractory state - can drive the resistant viral population to an observable transient viral rebound.

https://doi.org/10.1371/journal.ppat.1011680.g004

Recent studies provide evidence that SARS-CoV-2 -antibody immune complexes can infect and replicate in macrophages via interactions with FcγRIIA and FcγRIIIA receptors, or even via the complement component C1q receptor [91–95]. Based on these findings, we can hypothesize that if the virus-antibody immune complexes are not cleared at a sufficiently fast rate, their ability to infect additional cell types via ADE may allow the resistant strain to take over, leading to the observed transient viral rebound. However, data showing that ADE is important in SARS-CoV-2 infection in vivo is lacking and one recent study showed that although an infection-enhancing effect of human neutralizing antibodies was observed in vitro, the same neutralizing antibodies exhibited a protective effect in vivo, when infused into mice or macaques [96]. Another recent analysis using both in vitro and in vivo experiments involving BAM also found no support for it generating ADE of SARS-CoV-2 infection [97].

Two limitations of this study are that data for only 7 individuals was analyzed, and in several cases, the transition between sensitive and resistant virus was very quick, with no intermediate observations. However, this is the best data available to analyze viral rebound after BAM administration and provides enough data to explore the mechanisms we presented in our models. To ameliorate these issues, we used a mixed-effects fitting approach, which simultaneously fits all available data, thus increasing the robustness of the fitting results.

In this study, we tested the hypothesis that the generation of drug resistant variants coupled with an additional supply of target cells can lead to the observed transient viral rebound in

some persons with acute SARS-CoV-2 infection following treatment with BAM. Two models were formulated with different mechanisms that allow for the replenishment of target cells during the infection. By fitting the models to patient data, we showed that both models can explain the emergence of resistant virus associated with large transient viral rebounds of 3–4 logs. Comparison between the two models showed that the logistic proliferation model was slightly preferred based on BICc due to having fewer parameters to fit. Nevertheless, both mechanisms may be operational. We also found that variations in the target cell supply rate parameters have a strong impact on the magnitude of the viral rebound, which may explain why only some individuals develop observable transient resistant viral rebound. Finally, we highlighted the role of adaptive immunity in viral clearance in our models.

Supporting information

S1 Text. Supplemental material. Table A. Antibody concentration exponential decay rate estimated from A_{max} and A_{28}, where A_{28} is the antibody concentration at day 28. B2-7 does not have information on A_{max}, so the average A_{max} for the other 6 participants is used instead. The values for α and A_{max} are used in Eq (4). **Table B.** Fitting comparison using different estimates of γ relative to c. **Table C.** Definition, units and values of model parameters. Note that the subscripts 1, 2 for each parameter refers to the sensitive and resistant virus, respectively. If a fitted parameter is shared between the two models, the population estimate for the logistic proliferation model is reported first, followed by the innate immune response model. Values with $^{(*)}$ is the average of the estimated values for the seven participants. The values for k_{on} reported in Table S3 are in unit of $M^{-1}\ s^{-1}$, while the computation is done using a conversion to mL $\mu g^{-1} day^{-1}$ (see main text). **Fig A.** Fit of the target cell limited model with drug sensitive and resistant viral strain to the data. The circles represent viral load data, where filled green and red circles indicate viral populations dominated by either the sensitive or resistant viral strain, respectively. The unfilled circles are data below the limit of quantification or limit of detection (indicated by the two horizontal lines). Black curves are the best-fit of the model to the total viral load. The dashed–green or–red curves are model simulation of the sensitive or resistant viral strain, respectively. The first vertical red (dashed-dotted) line indicates the timing of treatment. The second vertical red (dashed) line indicates the estimated time when adaptive immunity begins to emerge. The dashed black curve shows the total viral load without treatment. **Fig B.** Long-term viral load in the logistic and innate immune response models without adaptive immunity. Simulations are done using the best fit parameters of participant B2-8 for both models. **Fig C.** Innate immune response model fit to data from patients who were treated with 700 mg BAM and did not rebound (part 1). The red bars indicate the limit of quantification (higher bar) and the limit of detection (lower bar). **Fig D.** Innate immune response model fit to data from patients who were treated with 700 mg BAM and did not rebound (part 2). The red bars indicate the limit of quantification (higher bar) and the limit of detection (lower bar). **Fig E.** Innate immune response model fit to data from control patients (part 1). The red bars indicate the limit of quantification (higher bar) and the limit of detection (lower bar). **Fig F.** Innate immune response model fit to data from control patients (part 2). The red bars indicate the limit of quantification (higher bar) and the limit of detection (lower bar). **Fig G.** Innate immune response model fit to data from control patients (part 3). The red bars indicate the limit of quantification (higher bar) and the limit of detection (lower bar). **Fig H.** Distributions of ρ and ϕ for rebound (n = 7) and non-rebound (n = 102) treated individuals with 700 mg BAM. Boxes in boxplots start in the first quartile and end in the third quartile of the data. The line is the median and the whiskers connect the top/bottom of the box to the max/min values that are not an outliers (data points further than 1.5 × IQR). Red crosses are outliers (outside

of the whisker range). **Fig I.** Distributions of ρ and ϕ for treated (700 mg BAM) rebound (n = 7) and placebo (n = 160) individuals. Boxes in boxplots start in the first quartile and end in the third quartile of the data. The line is the median and the whiskers connect the top/bottom of the box to the max/min values that are not an outliers (data points further than 1.5 × IQR). Red crosses are outliers (outside of the whisker range).
(DOCX)

Acknowledgments

The authors thank the study participants, site staff, site investigators, and the entire ACTIV-2/A5401 study team.

Author Contributions

Conceptualization: Tin Phan, Ruy M. Ribeiro, Ruian Ke, Alan S. Perelson.

Data curation: Kara W. Chew, Davey M. Smith, Eric S. Daar, David A. Wohl, Joseph J. Eron, Judith S. Currier, Michael D. Hughes, Manish C. Choudhary, Rinki Deo, Jonathan Z. Li.

Formal analysis: Tin Phan.

Funding acquisition: Ruy M. Ribeiro, Ruian Ke, Alan S. Perelson.

Investigation: Tin Phan, Carolin Zitzmann, Kara W. Chew, Davey M. Smith, Judith S. Currier, Michael D. Hughes, Manish C. Choudhary, Rinki Deo.

Methodology: Tin Phan, Ruy M. Ribeiro, Ruian Ke, Alan S. Perelson.

Project administration: Ruy M. Ribeiro, Ruian Ke, Alan S. Perelson.

Resources: Kara W. Chew, Davey M. Smith, Eric S. Daar, David A. Wohl, Joseph J. Eron, Judith S. Currier, Michael D. Hughes, Manish C. Choudhary, Rinki Deo, Jonathan Z. Li, Ruy M. Ribeiro, Ruian Ke, Alan S. Perelson.

Software: Tin Phan, Carolin Zitzmann.

Supervision: Ruy M. Ribeiro, Ruian Ke, Alan S. Perelson.

Validation: Tin Phan, Ruy M. Ribeiro, Ruian Ke, Alan S. Perelson.

Visualization: Tin Phan.

Writing – original draft: Tin Phan, Carolin Zitzmann, Ruy M. Ribeiro, Ruian Ke, Alan S. Perelson.

Writing – review & editing: Tin Phan, Carolin Zitzmann, Kara W. Chew, Jonathan Z. Li, Ruy M. Ribeiro, Ruian Ke, Alan S. Perelson.

References

1. COVID-19 Epidemiological Update - 29 September 2023. Available from: https://www.who.int/publications/m/item/covid-19-epidemiological-update—29-september-2023
2. Vaccine equity. Available from: https://www.who.int/campaigns/vaccine-equity
3. CDC. Coronavirus Disease 2019 (COVID-19). Centers for Disease Control and Prevention. 2020. Available from: https://www.cdc.gov/coronavirus/2019-ncov/variants/variant-classifications.html
4. Taylor PC, Adams AC, Hufford MM, de la Torre I, Winthrop K, Gottlieb RL. Neutralizing monoclonal antibodies for treatment of COVID-19. Nat Rev Immunol. 2021 Jun; 21(6):382–93. https://doi.org/10.1038/s41577-021-00542-x PMID: 33875867
5. Chew KW, Moser C, Daar ES, Wohl DA, Li JZ, Coombs RW, et al. Antiviral and clinical activity of bamlanivimab in a randomized trial of non-hospitalized adults with COVID-19. Nat Commun. 2022 Aug 22; 13(1):4931. https://doi.org/10.1038/s41467-022-32551-2 PMID: 35995785

6. Chen P, Nirula A, Heller B, Gottlieb RL, Boscia J, Morris J, et al. SARS-CoV-2 Neutralizing Antibody LY-CoV555 in Outpatients with Covid-19. N Engl J Med. 2021 Jan 21; 384(3):229–37. https://doi.org/10.1056/NEJMoa2029849 PMID: 33113295
7. Choudhary MC, Chew KW, Deo R, Flynn JP, Regan J, Crain CR, et al. Emergence of SARS-CoV-2 escape mutations during Bamlanivimab therapy in a phase II randomized clinical trial. Nat Microbiol. 2022 Oct 26; 7(11):1906–17. https://doi.org/10.1038/s41564-022-01254-1 PMID: 36289399
8. Jensen B, Luebke N, Feldt T, Keitel V, Brandenburger T, Kindgen-Milles D, et al. Emergence of the E484K mutation in SARS-COV-2-infected immunocompromised patients treated with bamlanivimab in Germany. Lancet Reg Health - Eur. 2021 Sep; 8:100164. https://doi.org/10.1016/j.lanepe.2021.100164 PMID: 34278371
9. Peiffer-Smadja N, Bridier-Nahmias A, Ferré VM, Charpentier C, Garé M, Rioux C, et al. Emergence of E484K Mutation Following Bamlanivimab Monotherapy among High-Risk Patients Infected with the Alpha Variant of SARS-CoV-2. Viruses. 2021 Aug 19; 13(8):1642. https://doi.org/10.3390/v13081642 PMID: 34452507
10. Boucau J, Chew KW, Choudhary MC, Deo R, Regan J, Flynn JP, et al. Monoclonal antibody treatment drives rapid culture conversion in SARS-CoV-2 infection. Cell Rep Med. 2022 Jul; 3(7):100678. https://doi.org/10.1016/j.xcrm.2022.100678 PMID: 35793677
11. Pantaleo G, Correia B, Fenwick C, Joo VS, Perez L. Antibodies to combat viral infections: development strategies and progress. Nat Rev Drug Discov. 2022 Sep; 21(9):676–96. https://doi.org/10.1038/s41573-022-00495-3 PMID: 35725925
12. Boucau J, Uddin R, Marino C, Regan J, Flynn JP, Choudhary MC, et al. Characterization of Virologic Rebound Following Nirmatrelvir-Ritonavir Treatment for Coronavirus Disease 2019 (COVID-19). Clin Infect Dis. 2023 Feb 8; 76(3):e526–9. https://doi.org/10.1093/cid/ciac512 PMID: 35737946
13. Carlin AF, Clark AE, Chaillon A, Garretson AF, Bray W, Porrachia M, et al. Virologic and Immunologic Characterization of Coronavirus Disease 2019 Recrudescence After Nirmatrelvir/Ritonavir Treatment. Clin Infect Dis. 2023 Feb 8; 76(3):e530–2. https://doi.org/10.1093/cid/ciac496 PMID: 35723411
14. Charness ME, Gupta K, Stack G, Strymish J, Adams E, Lindy DC, et al. Rebound of SARS-CoV-2 Infection after Nirmatrelvir–Ritonavir Treatment. N Engl J Med. 2022 Sep 15; 387(11):1045–7. https://doi.org/10.1056/NEJMc2206449 PMID: 36069968
15. Dai EY, Lee KA, Nathanson AB, Leonelli AT, Petros BA, Brock-Fisher T, et al. Viral Kinetics of Severe Acute Respiratory Syndrome Coronavirus 2 (SARS-CoV-2) Omicron Infection in mRNA-Vaccinated Individuals Treated and Not Treated with Nirmatrelvir-Ritonavir. Infectious Diseases (except HIV/AIDS); 2022 Aug. Available from: http://medrxiv.org/lookup/doi/10.1101/2022.08.04.22278378.
16. Ranganath N, O'Horo JC, Challener DW, Tulledge-Scheitel SM, Pike ML, O'Brien M, et al. Rebound Phenomenon After Nirmatrelvir/Ritonavir Treatment of Coronavirus Disease 2019 (COVID-19) in High-Risk Persons. Clin Infect Dis. 2023 Feb 8; 76(3):e537–9. https://doi.org/10.1093/cid/ciac481 PMID: 35698452
17. Stilianakis NI, Perelson AS, Hayden FG. Emergence of Drug Resistance during an Influenza Epidemic: Insights from a Mathematical Model. J Infect Dis. 1998 Apr 1; 177(4):863–73. https://doi.org/10.1086/515246 PMID: 9534957
18. Kepler TB, Perelson AS. Drug concentration heterogeneity facilitates the evolution of drug resistance. Proc Natl Acad Sci. 1998 Sep 29; 95(20):11514–9. https://doi.org/10.1073/pnas.95.20.11514 PMID: 9751697
19. Ribeiro RM, Bonhoeffer S. Production of resistant HIV mutants during antiretroviral therapy. Proc Natl Acad Sci. 2000 Jul 5; 97(14):7681–6. https://doi.org/10.1073/pnas.97.14.7681 PMID: 10884399
20. Rong L, Dahari H, Ribeiro RM, Perelson AS. Rapid Emergence of Protease Inhibitor Resistance in Hepatitis C Virus. Sci Transl Med. 2010 May 5; 2(30). Available from: https://www.science.org/doi/10.1126/scitranslmed.3000544. https://doi.org/10.1126/scitranslmed.3000544 PMID: 20445200
21. Ke R, Li H, Wang S, Ding W, Ribeiro RM, Giorgi EE, et al. Superinfection and cure of infected cells as mechanisms for hepatitis C virus adaptation and persistence. Proc Natl Acad Sci. 2018 Jul 24; 115(30). Available from: https://pnas.org/doi/full/10.1073/pnas.1805267115. https://doi.org/10.1073/pnas.1805267115 PMID: 29987026
22. Ke R, Zitzmann C, Ho DD, Ribeiro RM, Perelson AS. In vivo kinetics of SARS-CoV-2 infection and its relationship with a person's infectiousness. Proc Natl Acad Sci. 2021 Dec 7; 118(49):e2111477118. https://doi.org/10.1073/pnas.2111477118 PMID: 34857628
23. Cevik M, Tate M, Lloyd O, Maraolo AE, Schafers J, Ho A. SARS-CoV-2, SARS-CoV, and MERS-CoV viral load dynamics, duration of viral shedding, and infectiousness: a systematic review and meta-analysis. Lancet Microbe. 2021 Jan; 2(1):e13–22. https://doi.org/10.1016/S2666-5247(20)30172-5 PMID: 33521734

24. Killingley B, Mann AJ, Kalinova M, Boyers A, Goonawardane N, Zhou J, et al. Safety, tolerability and viral kinetics during SARS-CoV-2 human challenge in young adults. Nat Med. 2022 May; 28(5):1031–41. https://doi.org/10.1038/s41591-022-01780-9 PMID: 35361992

25. Ke R, Martinez PP, Smith RL, Gibson LL, Mirza A, Conte M, et al. Daily longitudinal sampling of SARS-CoV-2 infection reveals substantial heterogeneity in infectiousness. Nat Microbiol. 2022 Apr 28; 7 (5):640–52. https://doi.org/10.1038/s41564-022-01105-z PMID: 35484231

26. Zhang W, Wahl LM, Yu P. Viral Blips May Not Need a Trigger: How Transient Viremia Can Arise in Deterministic In-Host Models. SIAM Rev. 2014 Jan; 56(1):127–55.

27. Perelson AS, Ribeiro RM, Phan T. An explanation for SARS-CoV-2 rebound after Paxlovid treatment. Infectious Diseases (except HIV/AIDS); 2023 Jun. Available from: http://medrxiv.org/lookup/doi/10.1101/2023.05.30.23290747. https://doi.org/10.1101/2023.05.30.23290747 PMID: 37398088

28. Perelson AS, Ke R. Mechanistic Modeling of SARS-CoV-2 and Other Infectious Diseases and the Effects of Therapeutics. Clin Pharmacol Ther. 2021 Apr; 109(4):829–40. https://doi.org/10.1002/cpt.2160 PMID: 33410134

29. Cardozo-Ojeda EF, Duke ER, Peterson CW, Reeves DB, Mayer BT, Kiem HP, et al. Thresholds for post-rebound SHIV control after CCR5 gene-edited autologous hematopoietic cell transplantation. eLife. 2021 Jan 12; 10:e57646. https://doi.org/10.7554/eLife.57646 PMID: 33432929

30. Fang Y, Liu H, Huang H, Li H, Saqi A, Qiang L, et al. Distinct stem/progenitor cells proliferate to regenerate the trachea, intrapulmonary airways and alveoli in COVID-19 patients. Cell Res. 2020 Aug; 30 (8):705–7. https://doi.org/10.1038/s41422-020-0367-9 PMID: 32606347

31. Voigt EA, Swick A, Yin J. Rapid induction and persistence of paracrine-induced cellular antiviral states arrest viral infection spread in A549 cells. Virology. 2016 Sep; 496:59–66. https://doi.org/10.1016/j.virol.2016.05.019 PMID: 27254596

32. Wang S, Pan Y, Wang Q, Miao H, Brown AN, Rong L. Modeling the viral dynamics of SARS-CoV-2 infection. Math Biosci. 2020 Oct; 328:108438. https://doi.org/10.1016/j.mbs.2020.108438 PMID: 32771304

33. Hernandez-Vargas EA, Velasco-Hernandez JX. In-host Mathematical Modelling of COVID-19 in Humans. Annu Rev Control. 2020; 50:448–56. https://doi.org/10.1016/j.arcontrol.2020.09.006 PMID: 33020692

34. Gonçalves A, Bertrand J, Ke R, Comets E, de Lamballerie X, Malvy D, et al. Timing of Antiviral Treatment Initiation is Critical to Reduce SARS-CoV-2 Viral Load. CPT Pharmacomet Syst Pharmacol. 2020 Sep; 9(9):509–14.

35. Maisonnasse P, Aldon Y, Marc A, Marlin R, Dereuddre-Bosquet N, Kuzmina NA, et al. COVA1-18 neutralizing antibody protects against SARS-CoV-2 in three preclinical models. Nat Commun. 2021 Oct 20; 12(1):6097. https://doi.org/10.1038/s41467-021-26354-0 PMID: 34671037

36. Esmaeili S, Owens K, Wagoner J, Polyak SJ, Schiffer JT. A unifying model to explain nirmatrelvir / ritonavir's high efficacy during early treatment and low efficacy as post-exposure prophylaxis, and to predict viral rebound. Infectious Diseases (except HIV/AIDS); 2023 Aug. Available from: http://medrxiv.org/lookup/doi/10.1101/2023.08.23.23294505.

37. Kim KS, Ejima K, Iwanami S, Fujita Y, Ohashi H, Koizumi Y, et al. A quantitative model used to compare within-host SARS-CoV-2, MERS-CoV, and SARS-CoV dynamics provides insights into the pathogenesis and treatment of SARS-CoV-2. Sugden B, editor. PLOS Biol. 2021 Mar 22; 19(3):e3001128. https://doi.org/10.1371/journal.pbio.3001128 PMID: 33750978

38. Heitzman-Breen N, Ciupe SM. Modeling within-host and aerosol dynamics of SARS-CoV-2: The relationship with infectiousness. Yates AJ, editor. PLOS Comput Biol. 2022 Aug 1; 18(8):e1009997. https://doi.org/10.1371/journal.pcbi.1009997 PMID: 35913988

39. Perelson AS. Modelling viral and immune system dynamics. Nat Rev Immunol. 2002 Jan; 2(1):28–36. https://doi.org/10.1038/nri700 PMID: 11905835

40. Perelson AS, Neumann AU, Markowitz M, Leonard JM, Ho DD. HIV-1 Dynamics in Vivo: Virion Clearance Rate, Infected Cell Life-Span, and Viral Generation Time. Science. 1996 Mar 15; 271 (5255):1582–6. https://doi.org/10.1126/science.271.5255.1582 PMID: 8599114

41. Pawelek KA, Huynh GT, Quinlivan M, Cullinane A, Rong L, Perelson AS. Modeling Within-Host Dynamics of Influenza Virus Infection Including Immune Responses. Antia R, editor. PLoS Comput Biol. 2012 Jun 28; 8(6):e1002588. https://doi.org/10.1371/journal.pcbi.1002588 PMID: 22761567

42. Cardozo-Ojeda EF, Perelson AS. Modeling HIV-1 Within-Host Dynamics After Passive Infusion of the Broadly Neutralizing Antibody VRC01. Front Immunol. 2021 Aug 31; 12:710012. https://doi.org/10.3389/fimmu.2021.710012 PMID: 34531859

43. Chen RE, Winkler ES, Case JB, Aziati ID, Bricker TL, Joshi A, et al. In vivo monoclonal antibody efficacy against SARS-CoV-2 variant strains. Nature. 2021 Aug 5; 596(7870):103–8. https://doi.org/10.1038/s41586-021-03720-y PMID: 34153975

44. Liberti DC, Kremp MM, Liberti WA, Penkala IJ, Li S, Zhou S, et al. Alveolar epithelial cell fate is maintained in a spatially restricted manner to promote lung regeneration after acute injury. Cell Rep. 2021 May; 35(6):109092. https://doi.org/10.1016/j.celrep.2021.109092 PMID: 33979629

45. Bridges JP, Vladar EK, Huang H, Mason RJ. Respiratory epithelial cell responses to SARS-CoV-2 in COVID-19. Thorax. 2022 Feb; 77(2):203–9. https://doi.org/10.1136/thoraxjnl-2021-217561 PMID: 34404754

46. Samuel CE, Knutson GS. Mechanism of interferon action. Kinetics of decay of the antiviral state and protein phosphorylation in mouse fibroblasts treated with natural and cloned interferons. J Biol Chem. 1982 Oct; 257(19):11796–801. PMID: 6181060

47. Ulker N, Samuel CE. Mechanism of interferon action. II. Induction and decay kinetics of the antiviral state and protein P54 in human amnion U cells treated with gamma interferon. J Biol Chem. 1987 Dec; 262(35):16804–7. PMID: 2824506

48. Mizutani T, Fukushi S, Iizuka D, Inanami O, Kuwabara M, Takashima H, et al. Inhibition of cell proliferation by SARS-CoV infection in Vero E6 cells. FEMS Immunol Med Microbiol. 2006 Mar; 46(2):236–43. https://doi.org/10.1111/j.1574-695X.2005.00028.x PMID: 16487305

49. Avendaño-Ortiz J, Lozano-Rodríguez R, Martín-Quirós A, Maroun-Eid C, Terrón V, Valentín J, et al. Proteins from SARS-CoV-2 reduce T cell proliferation: A mirror image of sepsis. Heliyon. 2020 Dec; 6 (12):e05635. https://doi.org/10.1016/j.heliyon.2020.e05635 PMID: 33283062

50. Hekman RM, Hume AJ, Goel RK, Abo KM, Huang J, Blum BC, et al. Actionable Cytopathogenic Host Responses of Human Alveolar Type 2 Cells to SARS-CoV-2. Mol Cell. 2020 Dec; 80(6):1104–1122.e9. https://doi.org/10.1016/j.molcel.2020.11.028 PMID: 33259812

51. Saenz RA, Quinlivan M, Elton D, MacRae S, Blunden AS, Mumford JA, et al. Dynamics of Influenza Virus Infection and Pathology. J Virol. 2010 Apr 15; 84(8):3974–83. https://doi.org/10.1128/JVI.02078-09 PMID: 20130053

52. Lavielle M. Mixed effects models for the population approach: models, tasks, methods and tools. Boca Raton: Taylor & Francis; 2014. 365 p. (Chapman & Hall/CRC biostatistics series).

53. Burnham KP, Anderson DR. Practical Use of the Information-Theoretic Approach. In: Model Selection and Inference. New York, NY: Springer New York; 1998. p. 75–117. Available from: http://link.springer.com/10.1007/978-1-4757-2917-7_3.

54. Burnham KP, Anderson DR. Multimodel Inference: Understanding AIC and BIC in Model Selection. Sociol Methods Res. 2004 Nov; 33(2):261–304.

55. Ciupe SM, Tuncer N. Identifiability of parameters in mathematical models of SARS-CoV-2 infections in humans. Sci Rep. 2022 Aug 27; 12(1):14637. https://doi.org/10.1038/s41598-022-18683-x PMID: 36030320

56. Zitzmann C, Ke R, Ribeiro RM, Perelson AS. How robust are estimates of key parameters in standard viral dynamic models? PLoS Comput Biol. 2024; 20(4):e1011437. https://doi.org/10.1371/journal.pcbi.1011437

57. Néant N, Lingas G, Le Hingrat Q, Ghosn J, Engelmann I, Lepiller Q, et al. Modeling SARS-CoV-2 viral kinetics and association with mortality in hospitalized patients from the French COVID cohort. Proc Natl Acad Sci. 2021 Feb 23; 118(8):e2017962118. https://doi.org/10.1073/pnas.2017962118 PMID: 33536313

58. Lingas G, Néant N, Gaymard A, Belhadi D, Peytavin G, Hites M, et al. Effect of remdesivir on viral dynamics in COVID-19 hospitalized patients: a modelling analysis of the randomized, controlled, open-label DisCoVeRy trial. J Antimicrob Chemother. 2022 Apr 27; 77(5):1404–12. https://doi.org/10.1093/jac/dkac048 PMID: 35233617

59. Lauer SA, Grantz KH, Bi Q, Jones FK, Zheng Q, Meredith HR, et al. The Incubation Period of Coronavirus Disease 2019 (COVID-19) From Publicly Reported Confirmed Cases: Estimation and Application. Ann Intern Med. 2020 May 5; 172(9):577–82. https://doi.org/10.7326/M20-0504 PMID: 32150748

60. He X, Lau EHY, Wu P, Deng X, Wang J, Hao X, et al. Temporal dynamics in viral shedding and transmissibility of COVID-19. Nat Med. 2020 May 1; 26(5):672–5. https://doi.org/10.1038/s41591-020-0869-5 PMID: 32296168

61. Linton N, Kobayashi T, Yang Y, Hayashi K, Akhmetzhanov A, Jung S mok, et al. Incubation Period and Other Epidemiological Characteristics of 2019 Novel Coronavirus Infections with Right Truncation: A Statistical Analysis of Publicly Available Case Data. J Clin Med. 2020 Feb 17; 9(2):538. https://doi.org/10.3390/jcm9020538 PMID: 32079150

62. CDC. COVID-19 and Your Health. Centers for Disease Control and Prevention. 2020. Available from: https://www.cdc.gov/coronavirus/2019-ncov/symptoms-testing/symptoms.html

63. Hou YJ, Okuda K, Edwards CE, Martinez DR, Asakura T, Dinnon KH, et al. SARS-CoV-2 Reverse Genetics Reveals a Variable Infection Gradient in the Respiratory Tract. Cell. 2020 Jul; 182(2):429–446.e14. https://doi.org/10.1016/j.cell.2020.05.042 PMID: 32526206

64. Smith AP, Moquin DJ, Bernhauerova V, Smith AM. Influenza Virus Infection Model With Density Dependence Supports Biphasic Viral Decay. Front Microbiol. 2018 Jul 10; 9:1554. https://doi.org/10.3389/fmicb.2018.01554 PMID: 30042759

65. FACT SHEET FOR HEALTHCARE PROVIDERS: EMERGENCY USE AUTHORIZATION FOR PAXLOVID. U. S. Food and Drug Administration. Center for Drug Evaluation and Research.; 2023. Available from: https://www.fda.gov/media/155050/download.

66. Igarashi T, Brown C, Azadegan A, Haigwood N, Dimitrov D, Martin MA, et al. Human immunodeficiency virus type 1 neutralizing antibodies accelerate clearance of cell–free virions from blood plasma. Nat Med. 1999 Feb; 5(2):211–6. https://doi.org/10.1038/5576 PMID: 9930870

67. Amicone M, Borges V, Alves MJ, Isidro J, Zé-Zé L, Duarte S, et al. Mutation rate of SARS-CoV-2 and emergence of mutators during experimental evolution. Evol Med Public Health. 2022 Jan 5; 10(1):142–55. https://doi.org/10.1093/emph/eoac010 PMID: 35419205

68. Bar-On YM, Flamholz A, Phillips R, Milo R. SARS-CoV-2 (COVID-19) by the numbers. eLife. 2020 Apr 2; 9:e57309. https://doi.org/10.7554/eLife.57309 PMID: 32228860

69. Samuel CE. Antiviral Actions of Interferons. Clin Microbiol Rev. 2001 Oct; 14(4):778–809. https://doi.org/10.1128/CMR.14.4.778-809.2001 PMID: 11585785

70. García-Sastre A, Biron CA. Type 1 Interferons and the Virus-Host Relationship: A Lesson in Détente. Science. 2006 May 12; 312(5775):879–82.

71. Patil S, Fribourg M, Ge Y, Batish M, Tyagi S, Hayot F, et al. Single-cell analysis shows that paracrine signaling by first responder cells shapes the interferon-β response to viral infection. Sci Signal. 2015 Feb 10; 8(363). Available from: https://www.science.org/doi/10.1126/scisignal.2005728.

72. Gonçalves A, Maisonnasse P, Donati F, Albert M, Behillil S, Contreras V, et al. SARS-CoV-2 viral dynamics in non-human primates. Regoes RR, editor. PLOS Comput Biol. 2021 Mar 17; 17(3):e1008785. https://doi.org/10.1371/journal.pcbi.1008785 PMID: 33730053

73. Haun A, Fain B, Dobrovolny HM. Effect of cellular regeneration and viral transmission mode on viral spread. J Theor Biol. 2023 Feb; 558:111370. https://doi.org/10.1016/j.jtbi.2022.111370 PMID: 36460057

74. Fatehi F, Bingham RJ, Dykeman EC, Stockley PG, Twarock R. Comparing antiviral strategies against COVID-19 via multiscale within-host modelling. R Soc Open Sci. 2021 Aug; 8(8):210082. https://doi.org/10.1098/rsos.210082 PMID: 34430042

75. Hattaf K, Yousfi N, 1 Centre Régional des Métiers de l'Education et de la Formation (CRMEF), 20340 Derb Ghalef, Casablanca, Morocco, 2 Laboratory of Analysis, Modeling and Simulation (LAMS), Faculty of Sciences Ben M'sik, Hassan II University of Casablanca, P.O Box 7955 Sidi Othman, Casablanca, Morocco. Dynamics of SARS-CoV-2 infection model with two modes of transmission and immune response. Math Biosci Eng. 2020; 17(5):5326–40.

76. Chatterjee AN, Al Basir F. A Model for SARS-CoV-2 Infection with Treatment. Comput Math Methods Med. 2020 Sep 1; 2020:1–11.

77. Du SQ, Yuan W. Mathematical modeling of interaction between innate and adaptive immune responses in COVID-19 and implications for viral pathogenesis. J Med Virol. 2020 Sep; 92(9):1615–28. https://doi.org/10.1002/jmv.25866 PMID: 32356908

78. Li C, Xu J, Liu J, Zhou Y, School of Mathematics and Statistics, Xi'an Jiaotong University, Xi'an, 710049, China, School of Sciences, Xi'an University of Technology, Xi'an, 710048, China, et al. The within-host viral kinetics of SARS-CoV-2. Math Biosci Eng. 2020;17(4):2853–61.

79. Nikolaidis NM, Noel JG, Pitstick LB, Gardner JC, Uehara Y, Wu H, et al. Mitogenic stimulation accelerates influenza-induced mortality by increasing susceptibility of alveolar type II cells to infection. Proc Natl Acad Sci. 2017 Aug 8; 114(32). Available from: https://pnas.org/doi/full/10.1073/pnas.1621172114. https://doi.org/10.1073/pnas.1621172114 PMID: 28739896

80. Talemi SR, Höfer T. Antiviral interferon response at single-cell resolution. Immunol Rev. 2018 Sep; 285(1):72–80. https://doi.org/10.1111/imr.12699 PMID: 30129203

81. Jamilloux Y, Henry T, Belot A, Viel S, Fauter M, El Jammal T, et al. Should we stimulate or suppress immune responses in COVID-19? Cytokine and anti-cytokine interventions. Autoimmun Rev. 2020 Jul; 19(7):102567. https://doi.org/10.1016/j.autrev.2020.102567 PMID: 32376392

82. Padmanabhan P, Desikan R, Dixit NM. Modeling how antibody responses may determine the efficacy of COVID-19 vaccines. Nat Comput Sci. 2022 Feb 28; 2(2):123–31. https://doi.org/10.1038/s43588-022-00198-0 PMID: 38177523

83. Blanco-Melo D, Nilsson-Payant BE, Liu WC, Uhl S, Hoagland D, Møller R, et al. Imbalanced Host Response to SARS-CoV-2 Drives Development of COVID-19. Cell. 2020 May; 181(5):1036–1045.e9. https://doi.org/10.1016/j.cell.2020.04.026 PMID: 32416070

84. Bastard P, Rosen LB, Zhang Q, Michailidis E, Hoffmann HH, Zhang Y, et al. Autoantibodies against type I IFNs in patients with life-threatening COVID-19. Science. 2020 Oct 23; 370(6515):eabd4585. https://doi.org/10.1126/science.abd4585 PMID: 32972996

85. Bastard P, Gervais A, Le Voyer T, Rosain J, Philippot Q, Manry J, et al. Autoantibodies neutralizing type I IFNs are present in ~4% of uninfected individuals over 70 years old and account for ~20% of COVID-19 deaths. Sci Immunol. 2021 Aug 20; 6(62):eabl4340. https://doi.org/10.1126/sciimmunol.abl4340 PMID: 34413139

86. Rahimi P, Tarharoudi R, Rahimpour A, Mosayebi Amroabadi J, Ahmadi I, Anvari E, et al. The association between interferon lambda 3 and 4 gene single-nucleotide polymorphisms and the recovery of COVID-19 patients. Virol J. 2021 Dec; 18(1):221. https://doi.org/10.1186/s12985-021-01692-z PMID: 34775984

87. Zahid W, Farooqui N, Zahid N, Ahmed K, Anwar MF, Rizwan-ul-Hasan S, et al. Association of Interferon Lambda 3 and 4 Gene SNPs and Their Expression with COVID-19 Disease Severity: A Cross-Sectional Study. Infect Drug Resist. 2023 Oct;Volume 16:6619–28. https://doi.org/10.2147/IDR.S422095 PMID: 37840831

88. Israelow B, Song E, Mao T, Lu P, Meir A, Liu F, et al. Mouse model of SARS-CoV-2 reveals inflammatory role of type I interferon signaling. J Exp Med. 2020 Dec 7; 217(12):e20201241. https://doi.org/10.1084/jem.20201241 PMID: 32750141

89. Israelow B, Mao T, Klein J, Song E, Menasche B, Omer SB, et al. Adaptive immune determinants of viral clearance and protection in mouse models of SARS-CoV-2. Sci Immunol. 2021 Oct 29; 6(64): eabl4509.

90. Dong T, Liu G, Felce S, Yao X, Yin Z, Fries A, et al. Memory cytotoxic SARS-CoV-2 spike protein-specific CD4+ T cells associate with viral control. 2022 Feb. Available from: https://www.researchsquare.com/article/rs-1317569/v1.

91. Junqueira C, Crespo Â, Ranjbar S, De Lacerda LB, Lewandrowski M, Ingber J, et al. FcγR-mediated SARS-CoV-2 infection of monocytes activates inflammation. Nature. 2022 Jun 16; 606(7914):576–84.

92. Maemura T, Kuroda M, Armbrust T, Yamayoshi S, Halfmann PJ, Kawaoka Y. Antibody-Dependent Enhancement of SARS-CoV-2 Infection Is Mediated by the IgG Receptors FcγRIIA and FcγRIIIA but Does Not Contribute to Aberrant Cytokine Production by Macrophages. Schultz-Cherry S, editor. mBio. 2021 Oct 26; 12(5):e01987–21.

93. Okuya K, Hattori T, Saito T, Takadate Y, Sasaki M, Furuyama W, et al. Multiple Routes of Antibody-Dependent Enhancement of SARS-CoV-2 Infection. Medina RA, editor. Microbiol Spectr. 2022 Apr 27; 10(2):e01553–21. https://doi.org/10.1128/spectrum.01553-21 PMID: 35319248

94. Zhou Y, Liu Z, Li S, Xu W, Zhang Q, Silva IT, et al. Enhancement versus neutralization by SARS-CoV-2 antibodies from a convalescent donor associates with distinct epitopes on the RBD. Cell Rep. 2021 Feb; 34(5):108699. https://doi.org/10.1016/j.celrep.2021.108699 PMID: 33485405

95. Wu F, Yan R, Liu M, Liu Z, Wang Y, Luan D, et al. Antibody-dependent enhancement (ADE) of SARS-CoV-2 infection in recovered COVID-19 patients: studies based on cellular and structural biology analysis. Infectious Diseases (except HIV/AIDS); 2020 Oct. Available from: http://medrxiv.org/lookup/doi/10.1101/2020.10.08.20209114.

96. Li D, Edwards RJ, Manne K, Martinez DR, Schäfer A, Alam SM, et al. In vitro and in vivo functions of SARS-CoV-2 infection-enhancing and neutralizing antibodies. Cell. 2021 Aug; 184(16):4203–4219.e32.

97. Cross RW, Wiethoff CM, Brown-Augsburger P, Berens S, Blackbourne J, Liu L, et al. The Therapeutic Monoclonal Antibody Bamlanivimab Does Not Enhance SARS-CoV-2 Infection by FcR-Mediated Mechanisms. Pathogens. 2023 Nov 30; 12(12):1408. https://doi.org/10.3390/pathogens12121408 PMID: 38133292